1-15-2014

Observations of a Two-Layer Soil Moisture Influence on Surface Energy Dynamics and Planetary Boundary Layer Characteristics in a Semiarid Shrubland

Zulia Mayari Sanchez-Mejia
University of Arizona

Shirley A. Papuga
University of Arizona, shirley.papuga@wayne.edu

Recommended Citation

Sanchez-Mejia, Z. M., and S. A. Papuga (2014), Observations of a two-layer soilmoisture influence on surface energy dynamics and planetary boundary layer characteristics in a semiarid shrubland, *Water Resour. Res., 50*, 306–317, doi:10.1002/2013WR014135.

WATER RESOURCES RESEARCH, VOL. 50, 306–317, doi:10.1002/2013WR014135, 2014

Observations of a two-layer soil moisture influence on surface energy dynamics and planetary boundary layer characteristics in a semiarid shrubland

Zulia Mayari Sanchez-Mejia[1] and Shirley A. Papuga[1]

Received 17 May 2013; revised 22 September 2013; accepted 4 December 2013; published 15 January 2014.

[1] We present an observational analysis examining soil moisture control on surface energy dynamics and planetary boundary layer characteristics. Understanding soil moisture control on land-atmosphere interactions will become increasingly important as climate change continues to alter water availability. In this study, we analyzed 4 years of data from the Santa Rita Creosote Ameriflux site. We categorized our data independently in two ways: (1) wet or dry seasons and (2) one of the four cases within a two-layer soil moisture framework for the root zone based on the presence or absence of moisture in shallow (0–20 cm) and deep (20–60 cm) soil layers. Using these categorizations, we quantified the soil moisture control on surface energy dynamics and planetary boundary layer characteristics using both average responses and linear regression. Our results highlight the importance of deep soil moisture in land-atmosphere interactions. The presence of deep soil moisture decreased albedo by about 10%, and significant differences were observed in evaporative fraction even in the absence of shallow moisture. The planetary boundary layer height (PBL_h) was largest when the whole soil profile was dry, decreasing by about 1 km when the whole profile was wet. Even when shallow moisture was absent but deep moisture was present the PBL_h was significantly lower than when the entire profile was dry. The importance of deep moisture is likely site-specific and modulated through vegetation. Therefore, understanding these relationships also provides important insights into feedbacks between vegetation and the hydrologic cycle and their consequent influence on the climate system.

Citation: Sanchez-Mejia, Z. M., and S. A. Papuga (2014), Observations of a two-layer soil moisture influence on surface energy dynamics and planetary boundary layer characteristics in a semiarid shrubland, *Water Resour. Res.*, *50*, 306–317, doi:10.1002/2013WR014135.

1. Introduction

[2] The land surface and the atmosphere are tightly coupled through the exchange of energy and water [*Nicholson*, 2000; *Shukla and Mintz*, 1982; *Shuttleworth*, 1991]. Soil moisture plays an important role in this exchange [e.g., *Seneviratne et al*., 2010; *Vereecken et al*., 2008] through the partitioning of available energy into sensible and latent heating [*Brubaker and Entekhabi*, 1996; *Colby*, 1984]. Soil moisture control on the exchange of energy and water is especially strong in dryland ecosystems [*Small and Kurc*, 2003; *Vivoni et al*., 2008; *Williams and Albertson*, 2004]. Because over 40% of the Earth's land surface can be classified as arid to semiarid [e.g., *Okin et al*., 2009; *Reynolds et al*., 2007], understanding soil moisture control on the interactions between the land surface and the atmosphere will be critical for anticipating feedbacks associated with global change [*Betts*, 2000; *D'Odorico et al*., 2013; *Taylor et al*., 2002].

[3] Interest in the soil moisture influence on land-atmosphere interactions arises from observations of feedbacks between soil moisture and precipitation, where high rainfall may lead to increased soil moisture which, in turn, promotes increased rainfall, or where low rainfall may lead to a decrease in soil moisture, further decreasing rainfall [*Findell and Eltahir*, 1997; *Koster et al*., 2003]. One possible mechanism for this feedback is through direct contribution of surface moisture to precipitation through increased evapotranspiration (*ET*) [*Dekker et al*., 2007; *Dominguez et al*., 2008; *Eltahir and Bras*, 1996]. However, dry or wet soil conditions may also influence the surface energy budget and its relationship to the development of the planetary boundary layer (*PBL*) [*Betts et al*., 1996; *Eltahir*, 1998].

[4] Assuming no storage, the surface energy budget can be summarized as $R_n - G = LH + SH$, where R_n is the net radiation, G is the ground heat flux, LH is the latent heat flux, and SH is the sensible heat flux [*Pitman*, 2003].

Companion paper to *Sanchez-Mejia et al*. [2014] doi:10.1002/2013WR014150.

[1]School of Natural Resources and the Environment, University of Arizona, Tucson, Arizona, USA.

Corresponding author: S. A. Papuga, School of Natural Resources and the Environment, University of Arizona, Tucson, AZ 85719, USA. (papuga@email.arizona.edu)

0043-1397/14/10.1002/2013WR014135

The available energy, Q_a, is the amount of energy available for sensible and latent heat exchange with the atmosphere, i.e., $R_n - G$. The evaporative fraction (EF) is the fraction of Q_a that is partitioned into latent heating, i.e., LH/Q_a. The surface energy budget is coupled with the net radiation balance which can be summarized as $R_n = (SW_{in} - SW_{out}) + (LW_{in} - LW_{out}) = SW_{net} + LW_{net}$, where SW refers to shortwave radiation and LW refers to longwave radiation. Net shortwave radiation is influenced by the land surface through albedo, α, i.e., the amount of incoming shortwave radiation that is reflected. Net longwave radiation is influenced by the temperature and emissivity of the land surface.

[5] Multiple and complex interactions control land-atmosphere feedbacks [*Ek and Holtslag*, 2004]. For instance, the presence of soil moisture is expected to increase the EF [*Betts and Ball*, 1998; *Eltahir*, 1998]. Higher EF is expected to lower the land surface temperature and therefore outgoing longwave radiation [*Brubaker and Entekhabi*, 1996; *Eltahir*, 1998]. Further, an increase in ET associated with increased soil moisture should increase water vapor in the atmosphere, increasing the longwave radiation emitted back to the land surface [*Eltahir*, 1998; *Miller et al*., 2009]. Therefore, the combined effect of higher EF and higher ET should lead to a higher LW_{net} and therefore a lower planetary boundary layer height [*Santanello et al*., 2009]. Additionally, increased soil moisture should be associated with increased SW_{net} because wet soils tend to have a lower albedo than dry soils [*Cunnington and Rowntree*, 1986; *Small and Kurc*, 2003; *Twomey et al*., 1986]. This relationship is important in local soil moisture-albedo-precipitation feedbacks [*Zaitchik et al*., 2013]. Overall then, an increased R_n is expected with increase in surface soil moisture [*Eltahir*, 1998]; alternatively, an increase in emissivity may decrease R_n due to an increase of LW_{net} leaving the surface [*Pielke*, 1984]. Finally, because G is very small relative to R_n, an increased R_n is expected to increase the energy transported into the PBL by increasing Q_a [*Betts*, 2000; *Eltahir*, 1998; *Quinn et al*., 1995].

[6] These couplings between the land surface and the atmosphere have been shown to be especially strong in semiarid ecosystems [e.g., *Charney*, 1975]. Previous research has demonstrated the sensitivity of semiarid ecosystems to pulses of moisture [*Austin et al*., 2004; *Huxman et al*., 2004; *Loik et al*., 2004], i.e., concentrations of moisture that come in discrete surges. Pulses of moisture arrive either by frequent small storms that wet only the shallow surface layer or large but infrequent storms that wet deeper soil layers [*Kurc and Small*, 2007; *Sala and Lauenroth*, 1985; *Yaseef et al*., 2010]. How the layering of this soil moisture influences the partitioning of the vertical fluxes of energy and water in semiarid ecosystems is poorly understood.

[7] In semiarid ecosystems, Q_a increases as much as 80 W m^{-2} [*Kurc and Small*, 2004] with increasing soil moisture at the surface, a magnitude larger than changes in Q_a associated with major land surface changes such as deforestation [*Gash and Nobre*, 1997] or shrub encroachment [*Kurc and Small*, 2004]. Evaporation is also driven by moisture near the surface [*Cavanaugh et al*., 2011; *Kurc and Small*, 2004]. However, transpiration tends to be driven by the availability of soil moisture at depths greater than 20 cm, presumably delivered by large storms [*Cavanaugh et al*., 2011; *Domingo et al*., 1999; *Scott et al*., 2006; *Zeppel et al*., 2008]. Because transpiration and photosynthesis are inextricably linked, regardless of vegetation type, net ecosystem uptake of carbon dioxide also tends to occur only when moisture reaches depths greater than 20 cm [*Kurc and Small*, 2007; *Kurc and Benton*, 2010]. Further, analysis of time-lapse digital photography has demonstrated that green-up of creosotebush (*Larrea tridentata*), a widespread species in the Sonora, Chihuahua, and Mojave deserts, is also driven by moisture that reaches depths greater than 20 cm [*Kurc and Benton*, 2010]. These observations argue for the importance of the consideration of deep soil moisture in the cycling of energy and water, and therefore land-atmosphere interactions, in semiarid ecosystems.

[8] Based on the contrasting influence of shallow and deep soil moisture on surface energy dynamics in semiarid ecosystems, we have developed a paradigm for evaluating their relative roles in land-atmosphere interactions. Our objective is to evaluate how moisture in shallow (0–20 cm) and deep (20–60 cm) soil layers influences surface energy dynamics and planetary boundary layer characteristics. Specifically, we provide quantitative estimates of (1) the magnitude of changes in the surface energy budget associated with the presence or absence of soil moisture in each layer and (2) linkages between soil moisture in each layer and planetary boundary layer characteristics. This analysis is critical in assessing the importance of the inclusion of soil moisture in multiple soil layers in models of land-atmosphere interactions. Additionally, our results point to the consideration of size-of-storm in addition to timing and frequency when evaluating climate change impacts in semiarid ecosystems and their feedbacks to the atmosphere.

2. Study Area and Methods

2.1. Study Area

[9] Our study site is located within the Santa Rita Experimental Range (SRER) and is approximately 25 km south of Tucson, Arizona, USA. This site is co-located with the Santa Rita Creosote (US-SRC) Ameriflux eddy covariance site (http://ameriflux.ornl.gov) in the northern portion of the SRER (UTM: 12 R 515177, 3530284) at 950 m above sea level (Figure 1). With adherence to Ameriflux protocol, 30 min averaged CO_2, H_2O, and energy fluxes are calculated using 10 Hz measurements from an open path CO_2/H_2O infrared gas analyzer (LI-7500, LI-COR Inc., Lincoln, NE, USA) and a 3-D sonic anemometer (CSAT-3, Campbell Scientific Inc., Logan, UT, USA), both at 3.75 m. Data are stored in a CR5000 data logger (Campbell Scientific Inc., Logan, UT, USA) and downloaded every 2 weeks.

[10] Mean annual precipitation at the site is 294 mm (calculated from a 4 year record), more than 50% of which occurs from July to September; 89 years of precipitation record from a nearby station indicate that the long-term mean annual precipitation in the area is 255 mm (Northeast Station; http://ag.arizona.edu/SRER/data.html). Small rainfall events (<5 mm) are most frequent; however, events >20 mm make the largest contributions to the annual rainfall. As typical for the region, this site is characterized by a bimodal precipitation distribution. However, winter rains

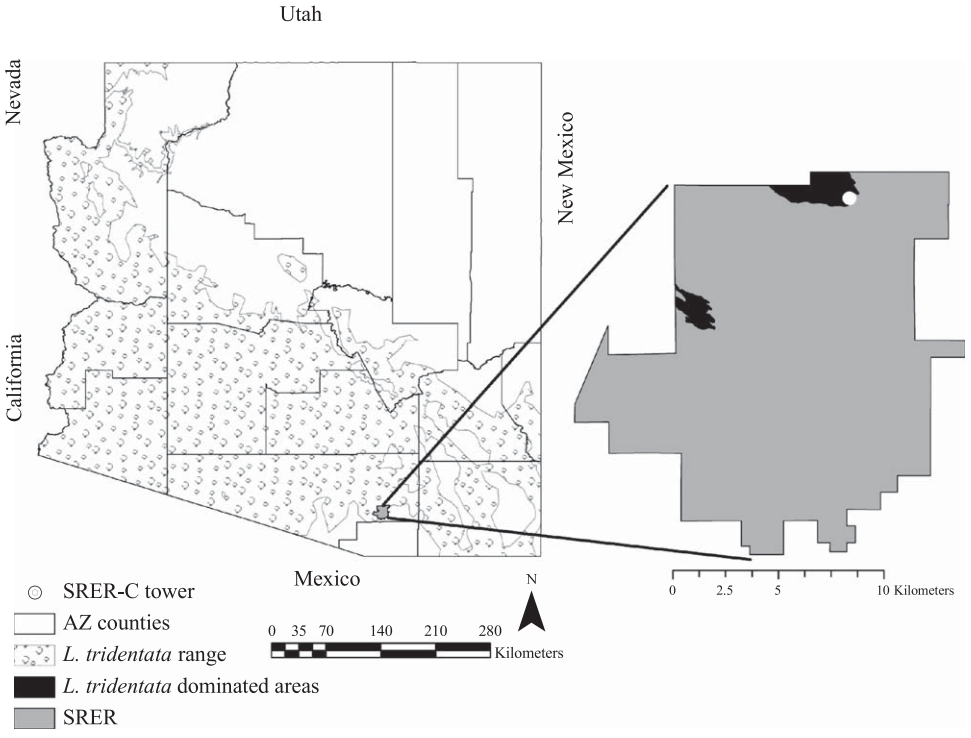

Figure 1. Location of study site. The Santa Rita Experimental Range (SRER) is shown in solid gray, and the white circle indicates the location of Santa Rita Creosote Ameriflux tower. The distribution range of *L. tridentata* is shown for Arizona in light gray semicircles, and the dominated areas in the SRER are shown in solid black.

(December, January, February) account only for ∼20% of the annual precipitation while precipitation in the months of July, August, and September accounts for about 60% of the annual precipitation. We define the monsoon season as "the shortest continuous period of the year during which 50% of the annual precipitation accumulates." To determine the monsoon for our study site, we analyzed long-term precipitation data from two stations within 1 km (Cholla and Northeast Stations; http://ag.arizona.edu/SRER/data.html). According to these data, the monsoon season occurs during the months of July, August, and September, hereafter referred to as the "wet season" (Day of Year (DOY) 182–273). The "dry season" (DOY 121–181) for this site occurs during the months of May and June (4% of total precipitation). Mean annual surface temperature is about 20°C, with monthly mean temperatures ranging from about 10°C during the winter to about 35°C during the summer.

[11] The physical landscape of the flux site is gently sloping (slopes <2%), and the soils are sandy-loam with a 10% increase of clay and silt from 35 to 75 cm depth. The site is a mosaic of canopy and bare patches; specifically, ∼14% are canopy patches of creosotebush (*Larrea tridentata*) and ∼86% are bare patches of which ∼8% host grasses, forbs, or cacti [*Kurc and Benton*, 2010]. The root distribution in the soil profile differs between bare and canopy patches; highest densities of roots are present at 10 and 35 cm in bare patches, while canopy patches have their highest density at 25 cm (Figure 2). These distributions were determined by excavating six 1 m soil pits, three in bare patches, and three in canopy patches, and extracting 10 cm × 10 cm soil samples every 5 cm. These soil samples were brought back to the laboratory, weighed, and then placed in a drying oven for 24 h at 60°C. After they were dried, they were reweighed. Following this drying, roots were collected through a tiered sieving process until no further roots could be identified with the naked eye. The collected roots were then weighed, and the root density was calculated as grams of roots per kilograms of dry soil.

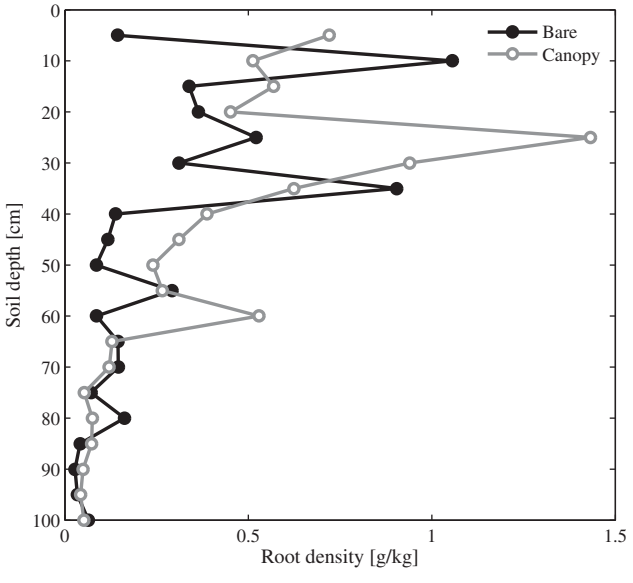

Figure 2. Root density (g/kg, root/soil) under bare (filled) and canopy (open). Each line represents the average from three independent profiles.

2.2. Data

[12] In this study, we present data from 2008 to 2011. In this section, we introduce how the data were collected and the instrumentation used. We also introduce how we calculate site-averaged values by combining measurements from bare soil patches and plant canopy patches. All surface and radiation variables were recorded every 30 min. Unless otherwise indicated, half-hour data were aggregated to a 24 h period starting at midnight local time. The flux tower was installed 2008 DOY = 72; data gaps (DOY 81–133 and 166–190 in 2008, DOY 154–159 in 2009, DOY 261–280 in 2010, DOY 30–34 in 2011) were caused by external disturbances to equipment or power failures.

2.2.1. Radiation and Surface Energy

[13] Incoming (SW_{in}) and outgoing (SW_{out}) shortwave radiations, as well as incoming (LW_{in}) and outgoing (LW_{out}) longwave radiations, are measured with a four-component net radiometer (CNR1, Kipp & Zonen, Inc., Delft, Netherlands) installed at 2.75 m above the surface and 10 m from the eddy covariance flux tower to avoid shading from other sensors. Net radiation (R_n) is calculated as $R_n = SW_{net} + LW_{net}$ where SW_{net} is the shortwave net radiation and LW_{net} is the longwave net radiation. Shortwave net radiation is calculated as the difference between SW_{in} and SW_{out}. Longwave net radiation is calculated as the difference between LW_{in} and LW_{out}.

[14] We corrected half-hour sensible and latent heat fluxes (*SH* and *LH*, respectively) collected from the data logger for an apparent flux occurring from density fluctuations [*Webb et al*., 1980]. We note that using eddy covariance sensible heat flux can only be measured to within 20% of its actual value. Because the sensible heat component of the surface energy budget can be very large in dryland ecosystems, we expect that the uncertainty in our *SH*, and therefore, our uncertainty in our correction for density fluctuations may also be very large. Finally, we established and used a friction velocity (u^*) threshold of 0.25 m s^{-1} [*Blanken et al*., 1998].

[15] Soil heat flux is measured at six locations (three canopy and three bare patches) using heat flux plates (HFP01SC, Hukseflux Thermal Sensors, Elektronicaweg, Netherlands) installed at a depth of 5 cm into the soil. Six soil temperature probes (TCAV-L50, Campbell Scientific Inc., Logan, UT, USA) are co-located with the heat flux plates. Ground heat flux (*G*), accounting for the storage of energy above the heat flux plates, is calculated from the soil heat flux and soil temperature using a combined calorimetric heat flux approach [*Kimball et al*., 1976; *Kurc and Small*, 2004].

[16] Surface albedo (α) is calculated as the ratio of outgoing to incoming shortwave radiation:

$$\alpha = \frac{SW_{out}}{SW_{in}} \tag{1}$$

[17] The available energy (Q_a) that could be transferred from the land surface to the atmosphere is calculated as

$$Q_a = R_n - G = LH + SH \tag{2}$$

[18] The evaporative fraction (*EF*) is the ratio of *LH* to Q_a, the fraction of available energy that is used toward latent heating, and is calculated as [*Shuttleworth*, 2012]

$$EF = \frac{LH}{SH + LH} \tag{3}$$

[19] Midday averages were calculated from 30 min data for α, Q_a, *EF*, and components of the surface energy budget. Midday averages (10:00 A.M. to 2:00 P.M., UTC/GMT-7, Mountain Standard Time, no daylight saving) are used because this is the time when available energy is at its maximum and incoming shortwave radiation is relatively stable.

2.2.2. Soil Moisture

[20] Six soil moisture profiles (under three bare and three canopy patches, not co-located with the soil heat flux plates) were monitored since 2008 using factory-calibrated water content reflectometers (CS616, Campbell Scientific Inc., Logan, UT, USA) at five different depths (2.5, 12.5, 22.5, 37.5, and 52.5). Average soil moisture at each depth calculated using the soil moisture from the profiles weighted based on the site-specific bare (86%) and canopy (14%) patch cover (equation (4)) [*Kurc and Small*, 2004; *Small and Kurc*, 2003]:

$$\theta = f\theta_C + (1-f)\theta_B \tag{4}$$

where θ is the volumetric soil moisture (m^3 m^{-3}) in the ecosystem, f is the fraction of canopy cover for the site, θ_C is the shrub canopy soil moisture, and θ_B is the bare ground soil moisture.

[21] Vertical moisture was aggregated into two different layers based on the relative influence of atmospheric demand, where the shallow layer (0–20 cm) is largely influenced by and the deep layer (20–60 cm) is minimally influenced by atmospheric demand. Weighted averages were based on the relative contribution of depth to the shallow (equation (5)) or deep (equation (6)) layers of the profile, and assuming each probe measures a source area with a radius of 7.5 cm:

$$\theta_{shallow} = 0.33\theta_{2.5} + 0.5\theta_{12.5} + 0.17\theta_{22.5} \tag{5}$$

$$\theta_{deep} = 0.25\theta_{22.5} + 0.375\theta_{37.5} + 0.375\theta_{52.5} \tag{6}$$

2.2.3. Atmospheric Sounding

[22] Atmospheric sounding data were obtained from the Department of Atmospheric Science, University of Wyoming (http://weather.uwyo.edu/upperair/sounding.html). The sounding data correspond to the National Weather Service surface Tucson station (KTUS, WMO: 72274) located at the Tucson International Airport (UTM: 12 R 504112, 3555012), which is about 29 km away from our study site. This means a single North American Regional Reanalysis grid cell would cover both our site and the airport. In this study, we analyzed the *PBL* characteristics using sounding data at 00 UTC which corresponds to a 5:00 P.M. local time.

[23] Planetary boundary layer height (PBL_h) was determined by analyzing potential temperature profiles (θ_p) [*Stull*, 1988]. In a mixed layer, θ_p remains constant with height; therefore, the height of the *PBL* can be determined using the gradient $\Delta\theta_p/\Delta z$ (Figure 3) in which θ_p is calculated as follows:

$$\theta_p = T\left(\frac{p_0}{p}\right)^{R/c_P} \tag{7}$$

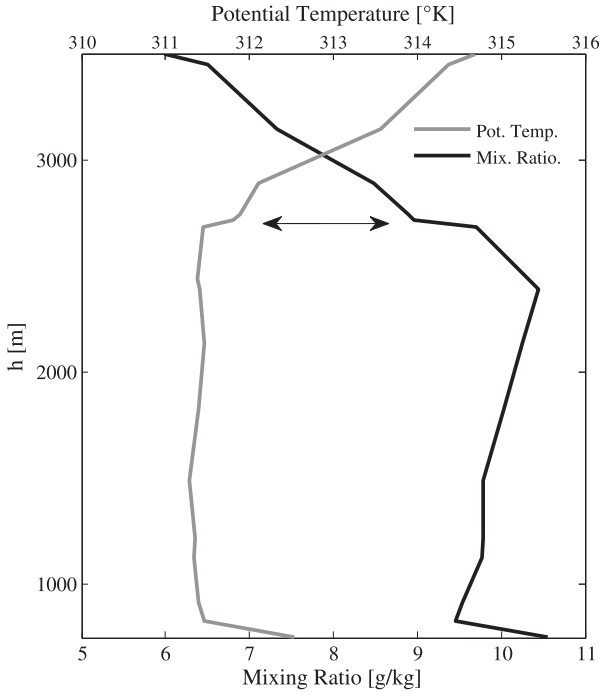

Figure 3. The planetary boundary height is established following the $\Delta\theta_P/\Delta h$ [*Stull*, 1988]. Here we present a typical profile from Case 1.

where θ_p (K) is the potential temperature, T (K) is the temperature at each level, p_0 (Pa) is the pressure at sea level, p (Pa) is the pressure at each level, R is assumed to be $\cong R_d = 287$ J K^{-1} kg^{-1} and $c_{pd} \cong 1004$ J K^{-1} kg^{-1}. We note that there are multiple ways to determine PBL_h and that the results can be sensitive to the method used [*LeMone et al*., 2013].

[24] An air parcel that travels from the surface adiabatically will reach a saturation point, i.e., the lifting condensation level (*LCL*, m), at which the temperature of the air parcel and dewpoint are equal). We can calculate the height of displacement from

$$T(z) = T_0 - \Gamma_d z \tag{8}$$

$$T_{dew}(z) = T_{dew0} - \Gamma_{dew} z \tag{9}$$

$$LCL = \frac{T_0 - T_{dew0}}{_d - \Gamma_{dew}} \tag{10}$$

where T_0 is the initial temperature, T_{dew0} is the initial dewpoint temperature, Γ_d is the dry adiabatic lapse rate, and Γ_{dew} is the dewpoint lapse rate. We assume a constant dry adiabatic lapse rate with height $\Gamma_d = 9.8$°C/km. T_{dew0} is calculated as

$$T_{dew0} = \frac{237.3\ \ln(e/0.6108)}{17.27 - \ln(e/0.6108)} \tag{11}$$

where T_{dew0} is in °C, and e is the actual vapor pressure [see *Wallace and Hobbs*, 2006], i.e.,

$$e = \frac{w}{w+\varepsilon} p \tag{12}$$

where w is the mixing ratio (g/kg), $\varepsilon = R_d/R_v = 0.622$, and p (kPa) is the pressure at the T level. Finally, Γ_{dew} is calculated as

$$\Gamma_{dew} = -\frac{dT_{dew}}{dz} = \frac{g}{\varepsilon l_v} \frac{T_{dew0}^2}{T_0} \tag{13}$$

where Γ_{dew} is in °C/km, g is 9.8 m s^{-2}, and lv is the latent heat of vaporization (2.5 $\times$ 10^6 J kg^{-1}), derived from Clausius-Clapeyron and Poisson's equation [*Tsonis*, 2007; *Wallace and Hobbs*, 2006].

[25] In addition, data available from the soundings include convective available potential energy (*CAPE*) and precipitable water (*PWAT*) for the whole sounding, a combination of which helps in understanding the likelihood of a thunderstorm. The *CAPE* is a measure of a potentially unstable atmosphere. It represents the potential energy available in an air parcel that can be transformed to kinetic energy in a buoyant updraft, i.e., *CAPE* >2500 J/kg supplies enough energy for strong updrafts and therefore thunderstorms [*Renno and Ingersoll*, 1996]. Precipitable water (*PWAT*) is an indicator of the moisture in the atmosphere. With enough *CAPE*, *PWAT* values above >30 mm generally suggest that thunderstorms are likely [*Kirkpatrick et al*., 2011; *Means*, 2012].

2.3. Soil Moisture Conceptual Framework

[26] Soil moisture drydown dynamics differ between the shallow and deep soil [*Cavanaugh et al*., 2011; *Kurc and Benton*, 2010], and therefore, two different approaches were used to define dry and wet periods in each layer (Figure 4a). For the shallow layer, soil moisture drydown curves were used to determine a moisture threshold. To do this, we first identified large storms, i.e., precipitation events >8 mm [*Sala and Lauenroth*, 1982]. Soil moisture values for the 14 days following each of the large precipitation events were used to develop an average drydown curve (Figure 4a). Then, an exponential model (equation (14)) was fit to this average drydown curve:

$$\theta(t) = (\theta_i - \theta_f) e^{(-t/\tau)} + \theta_f \tag{14}$$

where θ is the volumetric soil moisture (m^3 m^{-3}), t is the time in days from the rainfall event, θ_i is the soil moisture on the first day after the rainfall event, θ_f is the soil moisture on the last day of the drying curve, and τ is the exponential time constant [*Kurc and Small*, 2004; *Lohmann and Wood*, 2003; *Scott et al*., 1997]. Consistent with other studies, we identified the shallow soil moisture layer threshold as the time when one third of the moisture remained (i.e., at time τ) [*Kurc and Small*, 2004; *Lohmann and Wood*, 2003; *Scott et al*., 1997]. For our site this threshold occurred on day 4, when $\theta_{shallow}$ was 0.1229 (more than two significant digits are needed for this analysis). Therefore, the shallow layer was considered dry at moisture values less than 0.1229.

[27] The deep soil moisture threshold was determined by using carbon flux data from the eddy covariance tower, specifically using the net ecosystem exchange (*NEE*) of CO_2. In this approach, we assume that uptake of CO_2 (negative *NEE*) is an indicator of plant activity and that plant activity

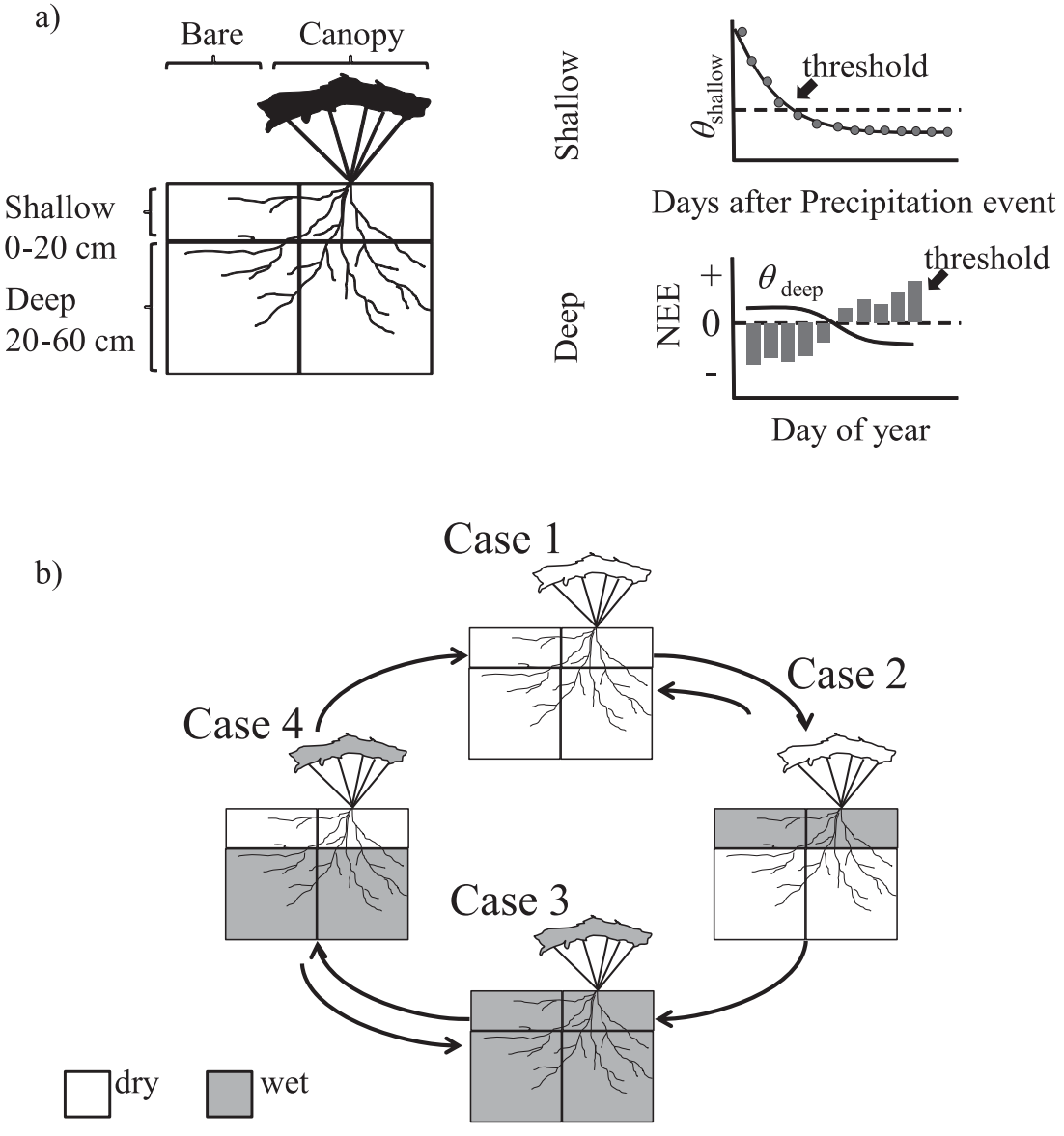

Figure 4. Our two-layer soil moisture conceptual framework. Soil moisture is influenced by its vertical distribution whether is at reach of atmospheric demand (0–20 cm) or not (20–60 cm). We use (a) a drydown curve to determine the soil moisture threshold in the shallow layer and a relationship between carbon uptake and soil moisture to determine the soil moisture threshold in the deep layer. (b) Using these thresholds, all days within the study period are categorized into cases, where Case 1 represents the dry state, Case 2 represents small precipitation events, Case 3 represents large precipitation events, and Case 4 represents drying of the surface after a large precipitation event.

only occurs when deep moisture is available for the plant to use [*Kurc and Small*, 2007]. For this threshold analysis, we selected a 10 day window in which *NEE* shifted from negative (uptake, five continuous days) to positive (release, five continuous days; Figure 4a). This transition signal indicated that low soil moisture levels in the deep layer were reducing photosynthetic activity. We assumed the fifth day of the positive *NEE* (release of CO_2) represented the time when soil moisture was unable to continue to support plant activity (Figure 4a); generally after 5 days, soil moisture was at a minimum. For our 4 year period (2008–2011) we extracted all 10 day windows that represented this transition and noted the soil moisture value on the fifth day of positive *NEE* for each; this resulted in a total of seven transition windows. To be conservative, we used the maximum value of the time series generated from soil moisture values on the fifth day (values had a range of 0.0858–0.1013). Therefore, the deep layer was considered dry at $\theta_{deep} < 0.1013$.

[28] These threshold values ($\theta_{shallow} = 0.1229$ and $\theta_{deep} = 0.1013$) were used to design the conceptual framework (Figure 4a) composed of four cases: (1) dry shallow soil ($\theta_{shallow} < 0.1229$) and dry deep soil ($\theta_{deep} < 0.1013$); (2) wet shallow soil ($\theta_{shallow} > 0.1229$) and dry deep soil ($\theta_{deep} < 0.1013$); (3) wet shallow soil ($\theta_{shallow} > 0.1229$) and wet deep soil ($\theta_{deep} > 0.1013$); and (4) dry shallow soil

($\theta_{shallow} < 0.1229$) and wet deep soil ($\theta_{deep} > 0.1013$; Figure 4b).

3. Results

[29] Here we demonstrate how soil moisture present or absent in shallow or deep soil layers influences land surface processes. We do this by analyzing (1) the surface energy budget components and (2) the planetary boundary layer characteristics, both in the context of our wet and dry seasons and in the context of our two-layer conceptual framework. Overall, our 4 year record consisted of 1227 days of micrometeorological observation and 1277 days of soil moisture observations. The four dry seasons total 244 days, while the four wet seasons total 368 days. Using our two-layer soil moisture framework which is not restricted to wet and dry seasons, days assigned to soil moisture cases were as follows: Case 1: 795 days (62%), Case 2: 18 days (1.4%), Case 3: 178 days (13.9%), and Case 4: 286 days (22.4%) .

3.1. Soil Moisture Influence on Radiation and Surface Energy Components

3.1.1. Wet and Dry Seasons

[30] When calculated using midday averages, differences in all radiation and surface energy components were statistically significant between the wet and dry seasons, with the exception of R_n and Q_a (Table 1). The similar average R_n between seasons is a result of higher average SW_{net} during the dry season and higher LW_{net} during the wet season (Table 1). The average midday ground heat flux G was positive during the dry season while negative during the wet season (Table 1). However, average midday G accounts for less than 4% of average midday R_n in either season which leads to a negligible difference between wet and dry seasons (Table 1). We note that the relatively low values for G (Table 1) are an artifact of the midday averaging period which did not capture the full G cycle.

[31] While overall, average SH was lower during the wet season than the dry season (Table 1), SH dominated the partitioning between SH and LH in both seasons. However, average LH was significantly higher during the wet season than the dry season by about 81 W m^{-2} (Table 1). Because the difference in average midday available energy Q_a was negligible between the seasons, this lower SH and higher LH leads to a significantly higher average midday EF during the wet season than the dry season (Table 1; Figure 5c).

[32] Average midday surface albedo was significantly higher during the dry season (0.192) than during the wet season (0.173; Table 1 and Figure 5a). This difference of 0.02 corresponds to about a 10% decrease in albedo under wet conditions.

3.1.2. Two-Layer Conceptual Framework

[33] When calculated using midday averages, differences in radiation and surface energy components were always statistically significant between conceptual framework cases the moisture state in the shallow layer differed, i.e., Cases 1 and 4 were always significantly different than Cases 2 and 3 (Table 1).

[34] Average R_n was lowest for Case 2, i.e., wet shallow layer and dry deep layer (Table 1). This was a result of significantly lower average SW_{net} for Case 2 than for the other cases (Table 1). The average midday ground heat flux G was positive for Cases 1 and 4 when the shallow layer was dry but negative for Cases 2 and 3 when the shallow layer was wet (Table 1). Similarly, average SH was significantly higher for Cases 1 and 4 when the shallow layer was dry

Table 1. Midday Average Values of Season and Case Analysis*

	Dry	Wet	Case 1	Case 2	Case 3	Case 4
n	244	368	795	18	178	286
R_n	510^{A}	515^{A}	444^{b}	296^{c}	410^{b}	490^{a}
SW_{net}	722^{A}	662^{B}	613^{a}	369^{c}	521^{b}	648^{a}
LW_{net}	-212^{B}	-147^{A}	-169^{b}	-73^{a}	-111^{a}	-158^{b}
G	18^{A}	-3^{B}	23^{a}	-6^{c}	-9^{c}	9^{b}
SH	286^{A}	213^{B}	232^{a}	113^{b}	139^{b}	220^{a}
LH	23^{B}	105^{A}	32^{c}	116^{a}	105^{a}	72^{b}
Q_a	526^{A}	508^{A}	467^{b}	290^{d}	400^{c}	499^{a}
α	0.193^{A}	0.173^{B}	0.182^{a}	0.167^{c}	0.163^{c}	0.174^{b}
EF	0.090^{B}	0.325^{a}	0.132^{c}	0.475^{a}	0.419^{a}	0.249^{b}

*Here we present net radiation (R_n, W m^{-2}), net shortwave radiation (SW_{net}, W m^{-2}), net longwave radiation (LW_{net}, W m^{-2}), ground heat flux (G, W m^{-2}), sensible heat flux (SH, W m^{-2}), latent heat flux (LH, W m^{-2}), available energy (Q_a, Wm^{-2}), albedo (α), and evaporative fraction (EF). Significance differences (t test, p value <0.01) are indicated by differences in superscript letter for season (A, B) and case (a, b, c, d). The number of days, n, is indicated under each category.

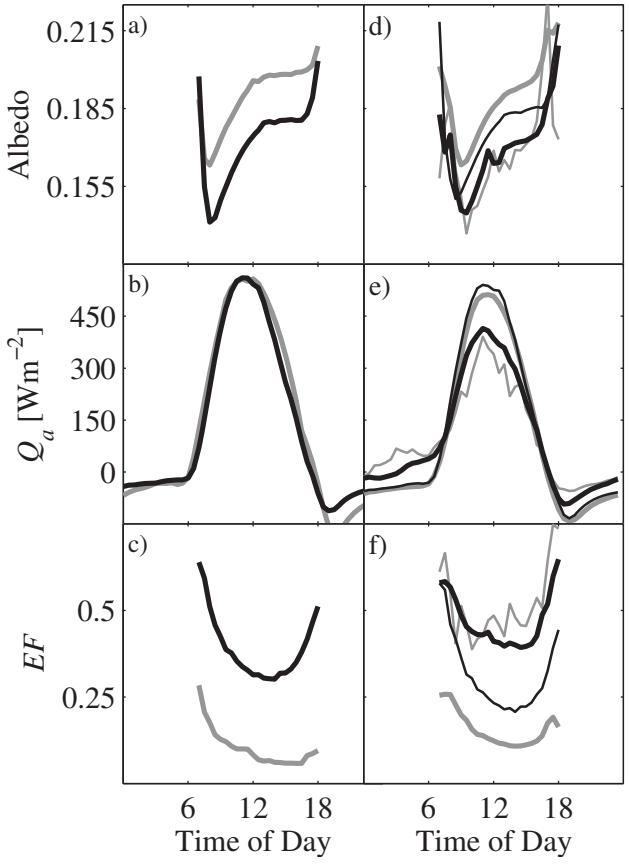

Figure 5. Average diurnal cycles of albedo, available energy (Q_a), and evaporative fraction (EF), by (a–c) season: wet (black line) and dry season (gray line) and by (d–f) case: Case 1 (thick gray line), Case 2 (thin gray line), Case 3 (thick black line), and Case 4 (thin black line).

than for Cases 2 and 3 when the shallow layer was wet (Table 1). As for wet and dry seasons, regardless of case, *SH* dominated the partitioning between *SH* and *LH*, with the exception of Case 2 where *LH* is slightly higher than *SH* (Table 1). Average *LH* was significantly higher for Cases 2 and 3 when the shallow layer was wet than for Cases 1 and 4 when the shallow layer was dry (Table 1).

[35] Average midday available energy Q_a was highest for Case 4 (499 W m^{-2}) when the deep layer was wet, but when the shallow layer was dry (Table 1 and Figure 5e). This is a consequence of R_n being largest for Case 4 (Table 1). Case 4 is likely under "drying" conditions with sparse cloud cover that may lead to the high SW_{net} (Table 1). Average midday available energy Q_a was lowest for Case 2 (290 W m^{-2}) when the shallow layer was wet but the deep layer was dry (Table 1 and Figure 5e). Again, in Case 2 R_n was lowest (Table 1). Because Case 2 is likely under short duration "wetting" conditions from a small storm before the surface has had time to dry, clouds likely lead to the low SW_{net} (Table 1). As a consequence, differences in Q_a were significant even when similar moisture conditions were present in the shallow layer (Table 1). Despite the differences in Q_a between the cases, Q_a did not appear to be strongly associated with increased soil moisture in either the shallow layer ($R^2 = 0.03$) or the deep layer ($R^2 = 0.01$; Figures 6e and 6f).

[36] *EF* was highest for Cases 2 (0.475) and 3 (0.419) when the shallow layer was wet (Table 1 and Figure 5f). While *EF* was lowest when the shallow layer was dry, *EF* was significantly higher for Case 4 than for Case 1 (Table 1 and Figure 5f), presumably because the moisture in the deep layer can be used for transpiration. *EF* tended to increase with increased soil moisture in either layer, but this association was stronger for the shallow ($R^2 = 0.66$) than for the deep soil layer ($R^2 = 0.32$; Figures 6c and 6d).

[37] Difference in albedo from a complete dry case (4) to wet case (3) is about 0.01 (Table 1 and Figure 5d); this corresponds to about a 9% decrease in albedo under wet conditions. Albedos for cases with any moisture at all (Cases 2, 3, 4) were significantly lower than for a completely dry soil profile (Case 1), even if this moisture was only present in the deep layer (Case 4; Table 1 and Figure 5d). Further, albedo tended to decrease with increased soil moisture in either layer, but this association was stronger for the shallow ($R^2 = 0.38$) than for the deep soil layer ($R^2 = 0.15$; Figures 6a and 6b).

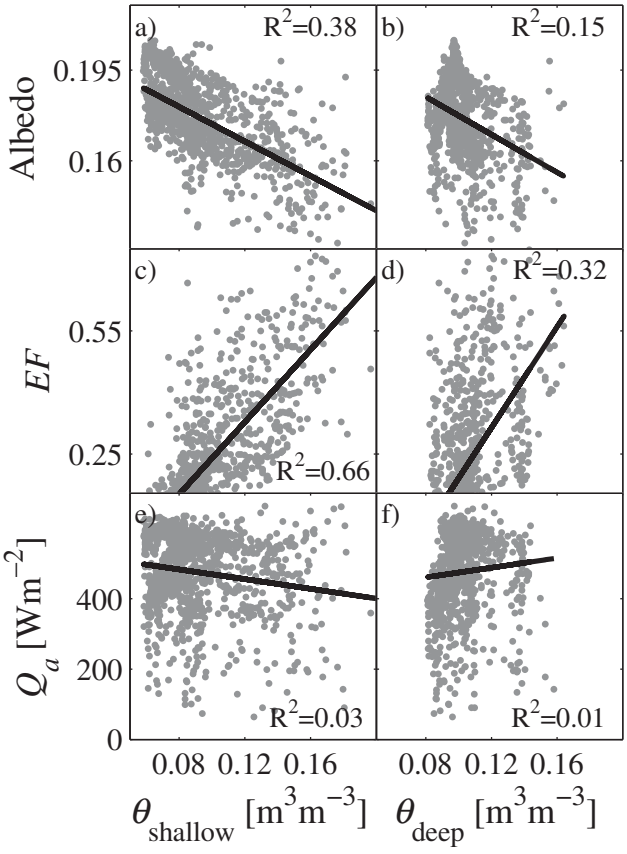

Figure 6. Linear regressions between: albedo and (a) shallow soil moisture ($\theta_{shallow}$) and (b) deep soil moisture (θ_{deep}); evaporative fraction (*EF*) and (c) shallow soil moisture and (d) deep soil moisture; and available energy (Q_a) and (e) shallow soil moisture and (f) deep soil moisture.

3.2. Soil Moisture Influence on the Planetary Boundary Layer

3.2.1. Wet and Dry Seasons

[38] Differences in all planetary boundary layer characteristics were statistically significant between the wet and dry seasons (Table 2). The PBL_h develops more during the dry season by a little more than 1 km (Table 2). In addition, the lifting condensation level (*LCL*) is more than 800 m higher in the dry season than the wet season (Table 2). During the dry season the *CAPE* is significantly lower than during the wet season (Table 2). Based on the average *CAPE* values, both the dry and wet season *PBL* values are likely to be "weak unstable," the range during the dry season goes from 0 to 24 J kg^{-1}, while during the wet season goes from 0 to 1280 J kg^{-1}. The *PWAT* is higher during the wet season than during the dry season by around 16 mm (Table 2). The wet season *PWAT* is 25 mm (Table 2) suggesting that thunderstorms are more likely in the wet season than the dry season.

3.2.2. Two-Layer Conceptual Framework

[39] The PBL_h was significantly lower when shallow layer was wet (Cases 2 and 3; Table 2). The PBL_h extended the most when the whole soil profile was dry (Case 1) and extended the least when the whole profile was wet (Case 3; Table 2). However, even when the shallow layer was dry but the deep layer was wet (Case 4), the height of the *PBL* was significantly lower than when the entire profile was dry (Case 1; Table 2). Further, the PBL_h tended to decrease with decreased albedo ($R^2 = 0.21$) under the presence of moisture, but this association was stronger for the shallow ($R^2 = 0.32$) than for the deep soil layer ($R^2 = 0.10$; Figure 7).

[40] The *LCL* was highest when whole soil profile was dry (Case 1) and was lowest when the shallow layer was wet (Cases 2 and 3; Table 2). Moisture in the deep layer tended to decrease the *LCL* whether or not moisture was present in the shallow layer (Case 4; Table 2). In general, the *CAPE* was lowest when the shallow layer was dry (Cases 1 and 4; Table 2). The *CAPE* was highest when the whole profile was wet (Case 3) and is statistically different

Table 2. The Planetary Boundary Layer Characteristics Analyzed Using a Two-Layer Soil Moisture Framework*

	Dry	Wet	Case 1	Case 2	Case 3	Case 4
n	32	32	32	11	32	32
PBL_h	3778^A	2550^B	2983^a	1969^c	1855^c	2592^b
LCL	4573^A	3705^B	4859^a	2797^c	2599^c	3503^b
CAPE	2^B	171^A	0^b	104^b	239^a	61^b
PWAT	9^B	25^A	6^c	30^a	33^a	20^b

*We present planetary boundary layer height (PBL_h, m), lifting condensation level (*LCL*, m), convective available potential energy (*CAPE*, J kg^{-1}), and precipitable water (*PWAT*, mm). Significance differences (*t* test, *p* value <0.01) are indicated by differences in superscript letter for season (A, B) and case (a, b, c, d). The number of days, *n*, is indicated under each category.

from other cases which were not statistically different from one another. *PWAT* was lowest when the entire soil profile was dry (Case 1) and highest when the entire soil profile was wet (Case 3; Table 2). Only in Case 3 *PWAT* was greater than 30 mm (Table 2), suggesting that thunderstorms are more likely under this soil moisture condition.

4. Discussion

[41] Our data demonstrate the importance of the presence of soil moisture on the surface energy dynamics in a semiarid shrubland and therefore its importance in modeling local land-atmosphere interactions. Consistent with previous theory [*Betts and Ball*, 1998; *Eltahir*, 1998], the presence of soil moisture was associated with an increase of *EF* (Table 1 and Figures 5c and 5f). However, our data also suggest that regardless of the moisture state of the shallow layer, a wet deep layer was associated with high *EF* (Figure 5f). This is most likely a consequence of the shrubs being able to access moisture in the deep layer for transpiration [*Cavanaugh et al*., 2011; *Zeppel et al*., 2008], even when moisture from the shallow layer is unavailable for latent heating. Also consistent with previous theory [*Eltahir*, 1998; *Miller et al*., 2009], higher LW_{net} was associated with the presence of soil moisture, as much as 60 W m^{-2} between wet and dry seasons (Table 1). In fact, LW_{net} was higher when the deep layer was wet but the shallow layer was dry (Case 4) than when the entire profile was dry (Case 1), though this difference was not significant (*t* test, $\alpha = 0.05$). Higher LW_{net} when the soil is moist may be a result of lower LW_{out} due to cooler soil, or a result of higher LW_{in} due to moist air and increased cloud cover.

[42] Consistent with previous studies [*Cunnington and Rowntree*, 1986; *Small and Kurc*, 2003; *Twomey et al*., 1986], albedo tended to be lower under wet conditions than dry conditions (Table 1 and Figure 5d). In fact, albedo was significantly lower when the deep layer was wet but the shallow layer was dry (Case 4) than when the entire profile was dry (Case 1). This suggests that moisture deep in the profile has an influence on the characteristics of the land surface. We suspect that because the shrubs have access to deep moisture through their roots, the moisture in the deep layer is altering the vegetation at the surface, which is altering the albedo. Supporting this notion, a recent study showed that in a semiarid shrubland, deep moisture, beyond the reach of atmospheric demand, is responsible for the greening of vegetation in these shrubland ecosystems [*Kurc and Benton*, 2010]. Because greening of vegetation influences albedo [*Asner*, 1998; *Berbert and Costa*, 2003; *Song*, 1999], the idea that deep soil moisture influences albedo is reasonable.

[43] Generally, despite lower albedos under wet conditions than dry conditions SW_{net} was higher under dry than wet conditions (Table 1), which was not expected [*Small and Kurc*, 2003]. This is likely a result of the use of a two-layer soil moisture conceptual framework to classify processes through time rather than looking for cloudy versus clear sky days. The use of cloudy days also has implications for the values of R_n. Contrary to expectations [*Eltahir*, 1998], our data show that R_n is not significantly different between wet and dry conditions, even between an entirely dry (Case 1) and an entirely wet (Case 3) soil profile (Table 1). These negligible differences in R_n associated with soil moisture are reflected in similar negligible differences in Q_a (Table 1). Therefore at our site, we did not observe the expected increase in Q_a associated with moisture-driven increase in R_n to increase the energy transported into the *PBL* [*Betts*, 2000; *Eltahir*, 1998; *Quinn et al*., 1995]. It is possible that these weak relationships could be explained with time-lagged associations between soil moisture states in the two layers and the surface energy dynamics and planetary boundary layer characteristics. Alternatively, changes

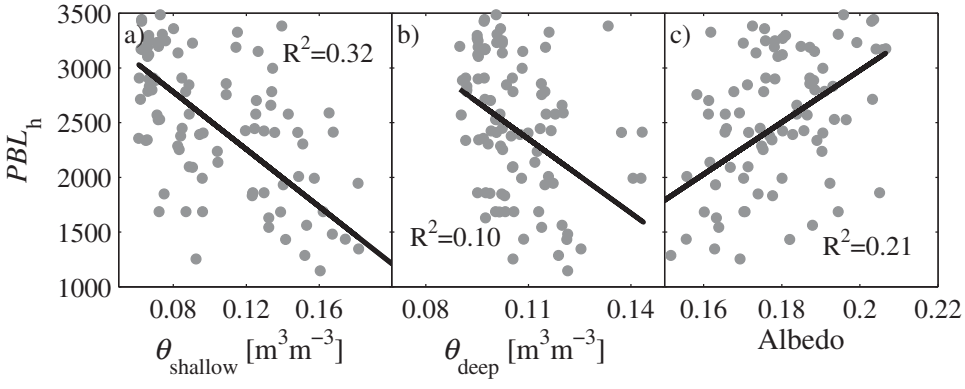

Figure 7. Linear regressions between the planetary boundary layer height and (a) shallow soil moisture ($\theta_{shallow}$), (b) deep soil moisture (θ_{deep}), and (c) albedo.

in *PBL* characteristics observed under different moisture conditions (Table 2) may be driven by other processes that are influenced by soil moisture. For instance, increased albedo (presumably by drying the soil) is associated with increased PBL_h (Figure 7c). Importantly, if moisture is present anywhere in the two layers, then *PBL* growth is significantly reduced. This has important implications for land-atmosphere feedbacks. Similarly, when the shallow layer is moist, the *LCL* is reduced considerably compared when the deep layer is moist (Table 2). This condition likely increases the relative humidity near the surface, which impacts evapotranspiration and ultimately the potential feedbacks between soil moisture and precipitation.

[44] Because the two-layer conceptual framework is based on thresholds influenced by wetting from precipitation pulses [*Sala and Lauenroth*, 1985], our data also demonstrate the importance of storm size and the consequent temporal dynamics of the "layering" of soil moisture associated with storm size on the surface energy components and planetary boundary layer characteristics. To summarize, for each day within our study period, the shrubland falls into a case (1–4; Figures 8e and 8j) based on the moisture states of a shallow and a deep layer (Figure 3b). Generally, before precipitation events both soil layers are dry (Case 1). After small precipitation events, the shallow layer is wetted, but the deep layer remains dry (Case 2; Figures 8a and 8f), after a larger precipitation event the deep layer is wetted in addition to the shallow layer (Case 3; Figures 8e and 8j). However, Case 3 is more persistent following larger storms (Figures 8a and 8f). Following both large and small storms, the surface energy budget is modified by a decrease in albedo (Figures 8d and 8i), an increase in *LH* (Figures 8c and 8h), and a decrease in *SH* (Figures 8c and 8h). These changes correspond to a shrinking of the *PBL* after both small and large precipitation events (Figures 8b and 8g). Importantly, the persistence of soil moisture in the deep layer through Case 3 and Case 4 (Figures 8e and 8j) is closely linked to the height of the *PBL* (Figures 8b and 8g) and the components of the surface energy budget (Figures 8c and 8h). This suggests that larger storms may have a greater influence on land-atmosphere interactions than small storms and that this influence is linked to the presence of deep soil moisture.

[45] Land-atmosphere interactions research has been improved by using continuous measurements of atmospheric and hydrological properties [e.g., *Baldocchi et al*., 2001; *Basara and Crawford*, 2002]. We link the importance of deep soil moisture to surface energy fluxes by showing linear relationships between variability in soil moisture at 20–60 cm depths and variability of multiple atmospheric properties. *Basara and Crawford* [2002] show the strength of the relationships between soil moisture and *SH*, *LH*, and *EF* especially with depths between 20 and 60 cm rather than at the surface. The results from our study highlight the importance of deep soil moisture in the consideration of land-atmosphere interactions.

[46] Insights from our research reflect the importance of considering the site-specific role of soil moisture for both shallow and deep layers of the root zone in land-atmosphere interactions. Because the mechanism by which deep soil moisture influences surface energy fluxes and planetary boundary characteristics is likely through transpiration [*Yaseef et al*., 2010], understanding site-specific controls on feedbacks between vegetation and the hydrologic cycle is critically important for land-atmosphere research [*Chahine*, 1992; *Dekker et al*., 2007; *Scheffer et al*., 2005]. For instance, root density with depth is likely important in the determination of the depth at which soil moisture most strongly influences surface energy dynamics. At our shrubland site, roots are concentrated at depths >20 cm (Figure 2),

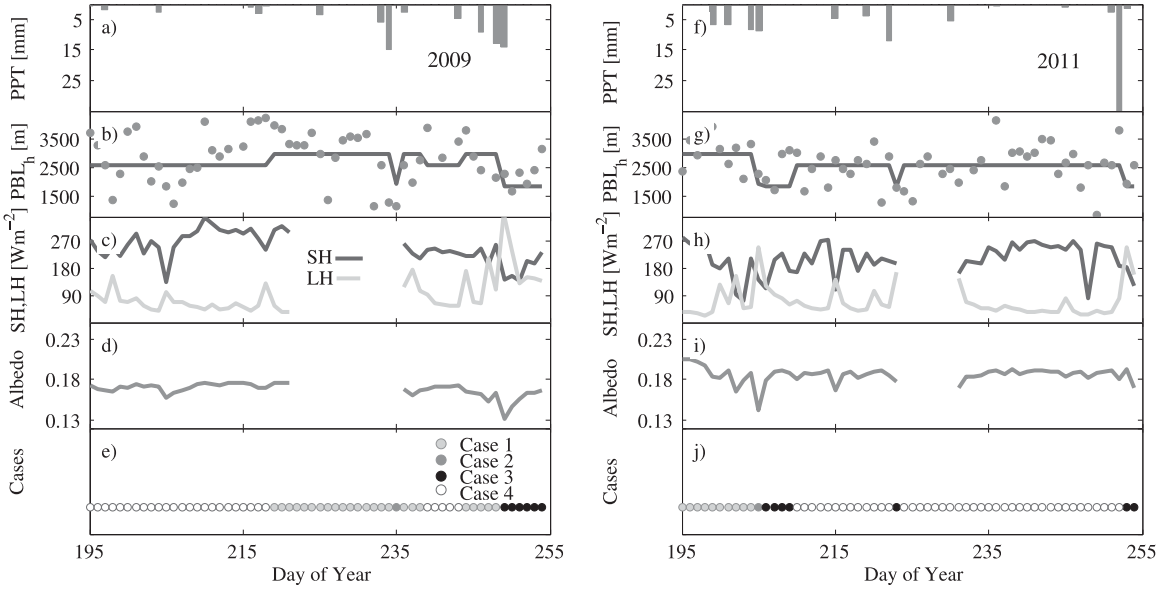

Figure 8. Summary showing two examples of (a, f) precipitation (*PPT*) events and how they are associated with (b, g) planetary boundary layer height (PBL_h) based on sounding data (dots) and based on case averages (line), (c, h) surface energy components' sensible heat (*SH*) and latent heat (*LH*) heat, (d, i) albedo, and (e, j) case over time as the soil dries.

and therefore, the strength of the relationship between moisture in the deep soil layer with radiation and surface energy components is reasonable. Furthermore, site-specific soil characteristics will also play a role in the layering of soil moisture and in the development of root density with depth [*Gregory et al*., 1987]. For instance, in desert ecosystems of the southwestern United States, a caliche layer, "bedrock," or a argilic horizon may inhibit root growth and soil moisture movement beyond depths of 40–60 cm [*Hennessy et al*., 1983].

[47] Additional sources of uncertainty must be considered in the interpretation of the surface energy dynamics. For instance, the temporal distribution of the cases is subject to variability in solar zenith angle throughout the year. Differences in solar zenith angle is likely to have a confounding effect on the albedo values for each case [*Wang et al*., 2005] as cases tended to be associated with particular times of year, e.g., Case 3 can occur during the monsoon season and in the presence of winter rains. Additionally, our two-layer framework does not discern between cloudy or clear sky days, which may add uncertainty to our findings. Clouds influence the incoming shortwave radiation and other surface energy components. While variations in albedo are not necessarily driven by cloud cover at local scales [*Small and Kurc*, 2003], at regional scales this may be an important source of uncertainty because cloud cover is not necessarily homogeneous [*van Leeuwen and Roujean*, 2002].

[48] Observational studies of land-atmosphere interactions are especially important (1) to better understand interactions and feedbacks and (2) for calibrating and validating land surface model (LSM) schemes. In this study, we focus on using these observations to quantify the influence of both shallow and deep soil moisture on the surface energy budget and *PBL* characteristics to contribute to the improvement of LSMs. We acknowledge that our study was limited to one study site and did not fully identify causality in the relationship between soil moisture and the surface energy budget and *PBL* characteristics. Despite these limitations, our study highlights the importance of these relationships in land-atmosphere interactions and suggests that more observational studies, at different temporal and spatial scales, are needed to further contribute to improving LSMs [*Santanello and Friedl*, 2003; *Santanello et al*., 2009, 2011].

[49] **Acknowledgments.** This research was supported in part by the University of Arizona College of Agriculture and Life Sciences (CALS), the Arizona University System Technology and Research Initiative Fund (TRIF), the University of Arizona Office of the Vice President for Research (VPR), SAHRA (Sustainability of semi-Arid Hydrology and Riparian Areas) under the STC Program of the National Science Foundation (NSF), NSF CAREER award EAR-1255013, and a doctoral studies fellowship provided through Mexican National Council for Science and Technology (CONACYT).

References

Asner, G. P. (1998), Biophysical and biochemical sources of variability in canopy reflectance, *Remote Sens. Environ.*, *64*(3), 234–253.

Austin, A. T., L. Yahdjian, J. M. Stark, J. Belnap, A. Porporato, U. Norton, D. A. Ravetta, and S. M. Schaeffer (2004), Water pulses and biogeochemical cycles in arid and semiarid ecosystems, *Oecologia*, *141*(2), 221–235.

Baldocchi, D., et al. (2001), FLUXNET: A new tool to study the temporal and spatial variability of ecosystem-scale carbon dioxide, water vapor, and energy flux densities, *Bull. Am. Meteorol. Soc.*, *82*(11), 2415–2434.

Basara, J., and K. Crawford (2002), Linear relationships between root-zone soil moisture and atmospheric processes in the planetary boundary layer, *J. Geophys. Res.*, *107*(D15), 4274, doi:10.1029/2001JD000633.

Berbert, M. L. C., and M. H. Costa (2003), Climate change after tropical deforestation: Seasonal variability of surface albedo and its effects on precipitation change, *J. Clim.*, *16*(12), 2099–2104.

Betts, A. K. (2000), Idealized model for equilibrium boundary layer over land, *J. Hydrometeorol.*, *1*(6), 507–523.

Betts, A. K., and J. H. Ball (1998), FIFE surface climate and site-average dataset 1987–89, *J. Atmos. Sci.*, *55*(7), 1091–1108.

Betts, A., J. Ball, A. Beljaars, M. Miller, and P. Viterbo (1996), The land surface-atmosphere interaction: A review based on observational and global modeling perspectives, *Journal of Geophysical Research-Atmospheres*, *101*(D3), 7209–7225.

Blanken, P. D., T. A. Black, H. H. Neumann, G. Den Hartog, P. C. Yang, Z. Nesic, R. Staebler, W. Chen, and M. D. Novak (1998), Turbulent flux measurements above and below the overstory of a boreal aspen forest, *Boundary Layer Meteorol.*, *89*(1), 109–140.

Brubaker, K. L., and D. Entekhabi (1996), Analysis of feedback mechanisms in land-atmosphere interaction, *Water Resour. Res.*, *32*(5), 1343–1357, doi:10.1029/96WR00005.

Cavanaugh, M., S. Kurc, and R. Scott (2011), Evapotranspiration partitioning in semiarid shrubland ecosystems: A two-site evaluation of soil moisture control on transpiration, *Ecohydrology*, *4*(5), 671–681.

Chahine, M. T. (1992), The hydrological cycle and its influence on climate, *Nature*, *359*(6394), 373–380.

Charney, J. G. (1975), Dynamics of deserts and drought in the Sahel, *Q. J. R. Meteorol. Soc.*, *101*(428), 193–202.

Colby, F. P. (1984), Convective inhibition as a predictor of convection during AVE-SESAME-II., *Mon. Weather Rev.*, *112*(11), 2239–2252.

Cunnington, W. M., and P. R. Rowntree (1986), Simulations of the Saharan atmosphere—Dependence on moisture and albedo, *Q. J. R. Meteorol. Soc.*, *112*(474), 971–999.

D'Odorico, P., A. Bhattachan, K. F. Davis, S. Ravi, and C. W. Runyan (2013), Global desertification: Drivers and feedbacks, *Adv. Water Resour.*, *51*, 326–344.

Dekker, S. C., M. Rietkerk, and M. F. P. Bierkens (2007), Coupling microscale vegetation-soil water and macroscale vegetation-precipitation feedbacks in semiarid ecosystems, *Global Change Biol.*, *13*(3), 671–678.

Domingo, F., L. Villagarcia, A. J. Brenner, and J. Puigdefabregas (1999), Evapotranspiration model for semi-arid shrub-lands tested against data from SE Spain, *Agric. For. Meteorol.*, *95*(2), 67–84.

Dominguez, F., P. Kumar, and E. R. Vivoni (2008), Precipitation recycling variability and ecoclimatological stability—A study using NARR data. Part II: North American monsoon region, *J. Clim.*, *21*(20), 5187–5203.

Ek, M., and A. Holtslag (2004), Influence of soil moisture on boundary layer cloud development, *J. Hydrometeorol.*, *5*(1), 86–99.

Eltahir, E. A. B. (1998), A soil moisture rainfall feedback mechanism: 1. Theory and observations, *Water Resour. Res.*, *34*(4), 765–776, doi:10.1029/97WR03499.

Eltahir, E. A. B., and R. L. Bras (1996), Precipitation recycling, *Rev. Geophys.*, *34*(3), 367–378, doi:10.1029/96RG01927.

Findell, K. L., and E. A. B. Eltahir (1997), An analysis of the soil moisture-rainfall feedback, based on direct observations from Illinois, *Water Resour. Res.*, *33*(4), 725–735, doi:10.1029/96WR03756.

Gash, J. H. C., and C. A. Nobre (1997), Climatic effects of Amazonian deforestation: Some results from ABRACOS, *Bull. Am. Meteorol. Soc.*, *78*(5), 823–830.

Gregory, P., J. Lake, and D. Rose (1987), *Root Development and Function*, 213 pp., Cambridge Univ. Press, New York, N. Y.

Hennessy, J. T., R. P. Gibbens, J. M. Tromble, and M. Cardenas (1983), Water properties of caliche, *J. Range Manage.*, *36*(6), 723–726.

Huxman, T. E., K. A. Snyder, D. Tissue, A. J. Leffler, K. Ogle, W. T. Pockman, D. R. Sandquist, D. L. Potts, and S. Schwinning (2004), Precipitation pulses and carbon fluxes in semiarid and arid ecosystems, *Oecologia*, *141*(2), 254–268.

Kimball, B. A., R. D. Jackson, R. J. Reginato, F. S. Nakayama, and S. B. Idso (1976), Comparison of field-measured and calculated soil-heat fluxes, *Soil Sci. Soc. Am. J.*, *40*(1), 18–25.

Kirkpatrick, C., E. W. McCaul, and C. Cohen (2011), Sensitivities of simulated convective storms to environmental CAPE, *Mon. Weather Rev.*, *139*(11), 3514–3532.

Koster, R. D., M. J. Suarez, R. W. Higgins, and H. M. Van den Dool (2003), Observational evidence that soil moisture variations affect

precipitation, *Geophys. Res. Lett.*, *30*(5), 1241, doi:10.1029/2002GL016571.

Kurc, S., and L. Benton (2010), Digital image-derived greenness links deep soil moisture to carbon uptake in a creosotebush-dominated shrubland, *J. Arid Environ.*, *74*(5), 585–594.

Kurc, S., and E. Small (2004), Dynamics of evapotranspiration in semiarid grassland and shrubland ecosystems during the summer monsoon season, central New Mexico, *Water Resour. Res.*, *40*, W09305, doi:10.1029/2004WR003068.

Kurc, S., and E. Small (2007), Soil moisture variations and ecosystem-scale fluxes of water and carbon in semiarid grassland and shrubland, *Water Resour. Res.*, *43*, W06416, doi:10.1029/2006WR005011.

LeMone, M. A., M. Tewari, F. Chen, and J. Dudhia (2013), Objectively determined fair-weather CBL depths in the ARW-WRF model and their comparison to CASES-97 observations, *Mon. Weather Rev.*, *141*(1), 30–54.

Lohmann, D., and E. F. Wood (2003), Timescales of land surface evapotranspiration response in the PILPS phase 2(c), *Global Planet. Change*, *38*(1–2), 81–91.

Loik, M. E., D. D. Breshears, W. K. Lauenroth, and J. Belnap (2004), A multi-scale perspective of water pulses in dryland ecosystems: Climatology and ecohydrology of the western USA, *Oecologia*, *141*(2), 269–281.

Means, J. D. (2012), GPS precipitable water as a diagnostic of the North American monsoon in California and Nevada, *J. Clim.*, *26*(4), 1432–1444.

Miller, R. L., A. Slingo, J. C. Barnard, and E. Kassianov (2009), Seasonal contrast in the surface energy balance of the Sahel, *J. Geophys. Res.—Atmos.*, *114*, D00E05, doi:10.1029/2008JD010521.

Nicholson, S. E. (2000), Land surface processes and Sahel climate, *Rev. Geophys.*, *38*(1), 117–139, doi:10.1029/1999RG900014.

Okin, G. S., A. J. Parsons, J. Wainwright, J. E. Herrick, B. T. Bestelmeyer, D. C. Peters, and E. L. Fredrickson (2009), Do changes in connectivity explain desertification?, *Bioscience*, *59*(3), 237–244.

Pielke, R. (1984), *Mesoscale Meteorological Modeling*, 673 pp., Academic Press, San Diego, Calif.

Pitman, A. J. (2003), The evolution of, and revolution in, land surface schemes designed for climate models, *Int. J. Climatol.*, *23*(5), 479–510.

Quinn, P., K. Beven, and A. Culf (1995), The introduction of macroscale hydrological complexity into land surface-atmosphere transfer models and the effect on planetary boundary layer development, *J. Hydrol.*, *166*(3–4), 421–444.

Renno, N. O., and A. P. Ingersoll (1996), Natural convection as a heat engine: A theory for CAPE, *J. Atmos. Sci.*, *53*(4), 572–585.

Reynolds, J. F., et al. (2007), Global desertification: Building a science for dryland development, *Science*, *316*(5826), 847–851.

Sala, O., and W. Lauenroth (1982), Small rainfall events: An ecological role in semiarid regions, *Oecologia*, *53*(3), 301–304.

Sala, O., and W. Lauenroth (1985), Root profiles and the ecological effect of light rainshowers in arid and semiarid regions, *Am. Midland Nat.*, *114*(2), 406–408.

Santanello, J., and M. Friedl (2003), Diurnal covariation in soil heat flux and net radiation, *J. Appl. Meteorol.*, *42*(6), 851–862.

Santanello, J., C. Peters-Lidard, S. Kumar, C. Alonge, and W. Tao (2009), A modeling and observational framework for diagnosing local land-atmosphere coupling on diurnal time scales, *J. Hydrometeorol.*, *10*(3), 577–599.

Santanello, J., C. Peters-Lidard, and S. Kumar (2011), Diagnosing the sensitivity of local land-atmosphere coupling via the soil moisture-boundary layer interaction, *J. Hydrometeorol.*, *12*(5), 766–786.

Scheffer, M., M. Holmgren, V. Brovkin, and M. Claussen (2005), Synergy between small- and large-scale feedbacks of vegetation on the water cycle, *Global Change Biol.*, *11*(7), 1003–1012.

Scott, R., D. Entekhabi, R. Koster, and M. Suarez (1997), Timescales of land surface evapotranspiration response, *J. Clim.*, *10*(4), 559–566.

Scott, R., T. Huxman, W. Cable, and W. Emmerich (2006), Partitioning of evapotranspiration and its relation to carbon dioxide exchange in a Chihuahuan Desert shrubland, *Hydrol. Processes*, *20*(15), 3227–3243.

Seneviratne, S. I., T. Corti, E. L. Davin, M. Hirschi, E. B. Jaeger, I. Lehner, B. Orlowsky, and A. J. Teuling (2010), Investigating soil moisture-climate interactions in a changing climate: A review, *Earth Sci. Rev.*, *99*(3–4), 125–161.

Shukla, J., and Y. Mintz (1982), Influence of land-surface evapo-transpiration on the Earth's climate, *Science*, *215*(4539), 1498–1501.

Shuttleworth, W. (1991), The Modellion concept, *Rev. Geophys.*, *29*(4), 585–606, doi:10.1029/91RG01815.

Shuttleworth, W. (2012), *Terrestrial Hydrometeorology*, 441 pp., Wiley-Blackwell, Oxford, U. K.

Small, E. E., and S. A. Kurc (2003), Tight coupling between soil moisture and the surface radiation budget in semiarid environments: Implications for land-atmosphere interactions, *Water Resour. Res.*, *39*(10), 1278, doi:10.1029/2002WR001297.

Song, J. (1999), Phenological influences on the albedo of prairie grassland and crop fields, *Int. J. Biometeorol.*, *42*(3), 153–157.

Stull, R. B. (1988), *An Introduction to Boundary Layer Meteorology*, 666 pp., Kluwer Acad. Publ., Boston.

Taylor, C. M., E. F. Lambin, N. Stephenne, R. J. Harding, and R. L. H. Essery (2002), The influence of land use change on climate in the Sahel, *J. Clim.*, *15*(24), 3615–3629.

Tsonis, A. (2007), *An Introduction to Atmospheric Thermodynamics*, 187 pp., Cambridge Univ. Press, New York, N. Y.

Twomey, S. A., C. F. Bohren, and J. L. Mergenthaler (1986), Reflectance and albedo differences between wet and dry surfaces, *Appl. Opt.*, *25*(3), 431–437.

van Leeuwen, W. J. D., and J. L. Roujean (2002), Land surface albedo from the synergistic use of polar (EPS) and geo-stationary (MSG) observing systems—An assessment of physical uncertainties, *Remote Sens. Environ.*, *81*(2–3), 273–289.

Vereecken, H., J. A. Huisman, H. Bogena, J. Vanderborght, J. A. Vrugt, and J. W. Hopmans (2008), On the value of soil moisture measurements in vadose zone hydrology: A review, *Water Resour. Res.*, *44*, W00D06, doi:10.1029/2008WR006829.

Vivoni, E. R., H. A. Moreno, G. Mascaro, J. C. Rodriguez, C. J. Watts, J. Garatuza-Payan, and R. L. Scott (2008), Observed relation between evapotranspiration and soil moisture in the North American monsoon region, *Geophys. Res. Lett.*, *35*, L22403, doi:10.1029/2008GL036001.

Wallace, J. M., and P. V. Hobbs (2006), *Atmospheric Science: An Introductory Survey*, Academic, London.

Wang, Z., M. Barlage, X. B. Zeng, R. E. Dickinson, and C. B. Schaaf (2005), The solar zenith angle dependence of desert albedo, *Geophys. Res. Lett.*, *32*, L05403, doi:10.1029/2004GL021835.

Webb, E. K., G. I. Pearman, and R. Leuning (1980), Correction of flux measurements for density effects due to heat and water vapour transfer, *Q. J. R. Meteorol. Soc.*, *106*(447), 85–100.

Williams, C. A., and J. D. Albertson (2004), Soil moisture controls on canopy-scale water and carbon fluxes in an African savanna, *Water Resour. Res.*, *40*, W09302, doi:10.1029/2004WR003208.

Yaseef, N. R., D. Yakir, E. Rotenberg, G. Schiller, and S. Cohen (2010), Ecohydrology of a semi-arid forest: Partitioning among water balance components and its implications for predicted precipitation changes, *Ecohydrology*, *3*(2), 143–154.

Zaitchik, B., J. Santanello, S. Kumar, and C. Peters-Lidard (2013), Representation of soil moisture feedbacks during drought in NASA unified WRF (NU-WRF), *J. Hydrometeorol.*, *14*(1), 360–367.

Zeppel, M., C. M. O. Macinnis-Ng, C. R. Ford, and D. Eamus (2008), The response of sap flow to pulses of rain in a temperate Australian woodland, *Plant Soil*, *305*(1–2), 121–130.